Journal of Colloid and Interface Science 498 (2017) 387–394

Contents lists available at ScienceDirect

Journal of Colloid and Interface Science

journal homepage: www.elsevier.com/locate/jcis

Regular Article

Facile microfluidic production of composite polymer core-shell microcapsules and crescent-shaped microparticles

Ekanem E. Ekanem, Zilin Zhang, Goran T. Vladisavljević *

Department of Chemical Engineering, Loughborough University, Loughborough LE11 3TU, United Kingdom

GRAPHICAL ABSTRACT

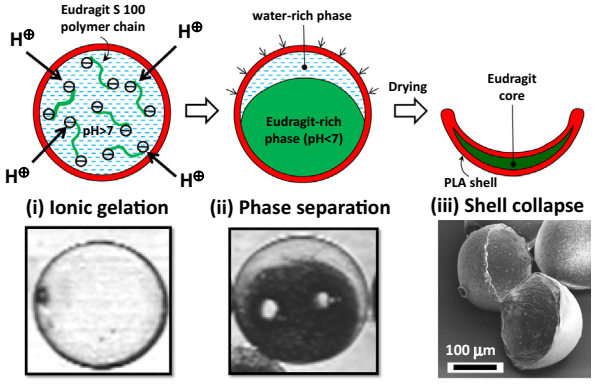

ARTICLE INFO

Article history:
Received 29 January 2017
Revised 14 March 2017
Accepted 15 March 2017
Available online 18 March 2017

Keywords:
Biodegradable polymers
Core-shell microcapsules
Eudragit
Cell encapsulation
Crescent particles
Ionic gelation
Microfluidics

ABSTRACT

Hypothesis: Core-shell microcapsules and crescent-shaped microparticles can be used as picolitre bioreactors for cell culture and microwells for cell trapping/immobilisation, respectively.
Results: Monodisperse polylactic acid (PLA) core-shell microcapsules with a diameter above 200 µm, a shell thickness of 10 µm, and 96% water entrapment efficiency were produced by solvent evaporation from microfluidically generated W/O/W emulsion drops with core-shell structure, and used to encapsulate *Saccharomyces cerevisiae* yeast cells in their aqueous cores. The morphological changes of the capsules stained with Nile red were studied over 14 days under different osmotic pressure and pH gradients.
Findings: The shell retained its integrity under isotonic conditions, but buckling and particle crumbling occurred in a hypertonic solution. When the capsules containing 5 wt% aqueous Eudragit® S 100 solution in the core were incubated in 10^{-4} M HCl solution, H^+ diffused through the PLA film into the core causing an ionic gelation of the inner phase and its phase separation into polymer-rich and water-rich regions, due to the transition of Eudragit from a hydrophilic to hydrophobic state. Crescent-shaped composite microparticles with Eudragit cores and PLA shells were fabricated by drying core-shell microcapsules with gelled cores, due to the collapse of PLA shells encompassing water-rich crescent regions.

1. Introduction

Microfluidic emulsification combined with solvent evaporation is a facile method for continuous production of monodispersed microparticles of versatile morphology and internal structure

* Corresponding author.
E-mail address: g.vladisavljevic@lboro.ac.uk (G.T. Vladisavljević).

http://dx.doi.org/10.1016/j.jcis.2017.03.067
0021-9797/

including non-spherical particles, e.g. crescent-moon-shaped [1], dendritic [2], and toroidal [3], surface-patterned particles with surface patches [4] and dimples [5], microcapsules composed of controlled number of inner compartments such as multi-compartment colloidosomes [6], polymersomes [7], and liposomes [8], and asymmetric particles with spatially segregated sections, such as Janus [9] and ternary [10] particles. Alternative fabrication methods, such as masking/unmasking techniques [11], microcontact printing, layer-by-layer deposition [12], internal phase separation, and direct polymerisation [13], are typically batch-wise, involve complex and multi-step processing, specific formulations and lead to poor particle size uniformity. The particles produced by microfluidic routes are monodispersed and their size and morphology can be controlled by changing the size and morphology of the parent drops. Glass capillary microfluidic devices are increasingly used for manufacturing microparticles [14–16], due to their 3D geometry, cheap fabrication process, ability to generate complex droplets in single emulsification step, and excellent optical properties and chemical resistance of borosilicate glass. Furthermore, glass surface can be readily functionalized to tailor its surface wettability.

Hydrogel microbeads are difficult to produce in microfluidic devices because the drop pinch-off must be decoupled from the gelation process to avoid clogging of the channels. However, typical ionic reactions that occur during ionotropic gelation are much faster than the drop generation. To overcome this problem, gel beads were produced in microfluidic systems by coalescence-induced gelation [17], chaotic mixing [18], competitive ligand exchange crosslinking [19], internal gelation using calcium or barium carbonate nanoparticles dispersed in the aqueous phase and acidified oil phase [20], and external gelation using the oil phase containing $CaCl_2$ [21–23]. These fabrication routes usually result in the formation of coherent gel microcapsules with uniform internal structure.

Composite microcapsules with gelled shells and oily cores were fabricated in microfluidic systems using O/W/O emulsions as templates [24,25]. Microcapsules with gelled shells and aqueous cores were fabricated via W/W/O emulsions and used for encapsulation of carcinoma cells [22]. To the best of our knowledge microcapsules with gelled cores and biodegradable polymer shells have not yet been generated by microfluidic methods.

Crescent-moon-shaped polymer particles were obtained by polymerisation of microfluidically emulsified Janus droplets composed of non-curable phase and photocurable phase [4,26] selective polymer leaching from acorn-shaped Janus particles [27], and non-uniform solvent evaporation from Janus droplets [28].

In this study, novel core-shell microcapsules with gelled or non-gelled aqueous cores and biodegradable polymer shells were fabricated and used as templates for composite crescent microparticles. The fabrication method is based on single-step microfluidic generation of core-shell W/O/W emulsion droplets, followed by solvent evaporation and an off-chip ionic gelation of a pH-sensitive, biocompatible polymer in the core. The fabricated microcapsules with aqueous cores were loaded with yeast cells to demonstrate high encapsulation efficiency of the fabrication method. In addition, morphological changes of the fabricated microcapsules over prolonged storage were investigated under different incubation conditions.

2. Materials and methods

2.1. Droplet generation and microparticle production

Core-shell drops were generated using glass capillary device with a combined co-flow/counter-current flow focusing geometry shown in Fig. 1. The device was fabricated and operated using the procedures described elsewhere [29,30]. The middle fluid was a mixture of 7 wt% PLA (poly(dl-lactic acid), M_w = 89,000 g/mol, IngeoTM 2060D) and 2 wt% PGPR (polyglycerol polyricinoleate, E476, Abitec Ltd., New Milton, UK) in DCM (dichloromethane, HPLC grade, Fisher Scientific, UK). Nile red (9-diethylamino-5-benzo[α] phenoxazinone, Sigma-Aldrich, UK) was added in the trace amounts as a lipophilic stain to visualize PLA shells by fluorescence microscopy after DCM evaporation. The inner fluid was pure water prepared using a Millipore 185 Milli-Q Plus water purification system or 5 wt% aqueous solution of Eudragit® S 100 (methacrylic acid-methyl methacrylate copolymer 1:2, Evonik, Germany) dissolved in 0.1 M NaOH. Eudragit® S 100 is soluble at pH ≥ 7 and precipitates at pH < 7. The continuous fluid was 5 wt% aqueous solution of PVA (poly(vinyl alcohol), M_w = 13,000–23,000 g/mol, 87–89% hydrolysed, Sigma-Aldrich).

At optimum fluid flow rates, monodispersed single core or dual-core drops were generated, as shown in Fig. 1 and Videos 1 and 2 in the supplementary material. Monodispersed core-shell particles with thin PLA shells and aqueous cores were produced upon DCM evaporation from the middle phase. A pH-triggered gelation of an aqueous Eudragit® S 100 solution from the cores was achieved by incubating the core-shell particles in the acidic environment. Finally, the capsules with gelled cores were collapsed by drying-induced buckling under ambient conditions to produce crescent-shaped microparticles with Eudragit core and PLA shell.

2.2. Confocal fluorescence microscopy

A drop of the particle suspension was placed on a microscope slide and allowed to dry. As a result of the inclusion of Nile red dye in the middle phase formulation, hydrophobic regions of the produced particles were fluorescent and visualized using a Nikon Eclipse TE300 confocal inverted microscope connected to a computer running Zeiss LaserSharp 2000 software. Nile red was excited with argon laser at a wavelength of 488 nm and helium-neon laser at 543 nm. The total emission was divided into two wavelength regions, detected by two photomultiplier tubes (PMTs): PMT1 captured fluorescence at 515 ± 30 nm (the green region) and PMT2 captured fluorescence above 570 nm (the red region). Only PMT2 images are presented in this work. Corresponding optical images of microparticles were simultaneously acquired using the same microscope.

2.3. Focused ion beam (FIB) imaging

To avoid particle distortion and disruption due to high beam energy, 2 kV was used throughout. External imaging of the particle was performed at 30 pA and a tilt angle of 52° before a protective platinum layer was deposited at 0.3 nA. If needed, the particle cross section was milled at 20 nA and cleaned at 7 nA, followed by the final cleaning at 3 nA. Finally, the current was reduced to 30 pA to preserve the exposed cross section and prevent its modification due to exposure to ion beam during imaging, which was carried out at 2 min/image for noise reduction.

2.4. Prediction of particle size

Fig. 2a shows the two extreme morphological transformations of a core-shell drop during solvent evaporation from the shell, Path A and B, where 0% and 100% core-water entrapment scenarios are depicted respectively.

The diameter of the particle formed via path A depends on the density of the dispersed phase, ρ_d prior to solvent evaporation, the density of the formed particle, ρ_p, the mass fraction x_p of the

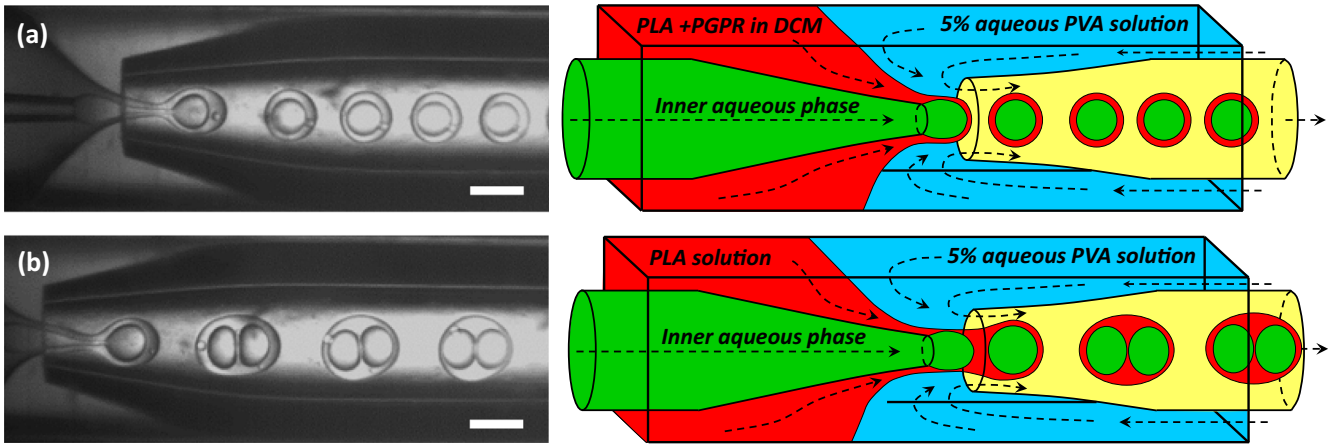

Fig. 1. Droplet generation using cocurrent/countercurrent flow focusing streams in coaxial assemblies of glass capillaries: (a) Single core microdroplets: (b) Dual core microdroplets. Volumetric flow rates of inner phase (Q_i), middle phase (Q_m), and continuous phase (Q_c) are: (a) 1 mL/h, 2 mL/h, and 10 mL/h respectively; and (b) 1.5 mL/h, 2.5 mL/h, and 10 mL/h respectively. Diameters of the droplet (D_d), inner core (D_i), injection nozzle (D_N) and collection capillary orifice (D_c) are: (a) 308 μm, 207 μm, 100 μm and 350 μm respectively; and (b) 418 μm, 225 μm, 100 μm and 350 μm. Scale bars: 300 μm.

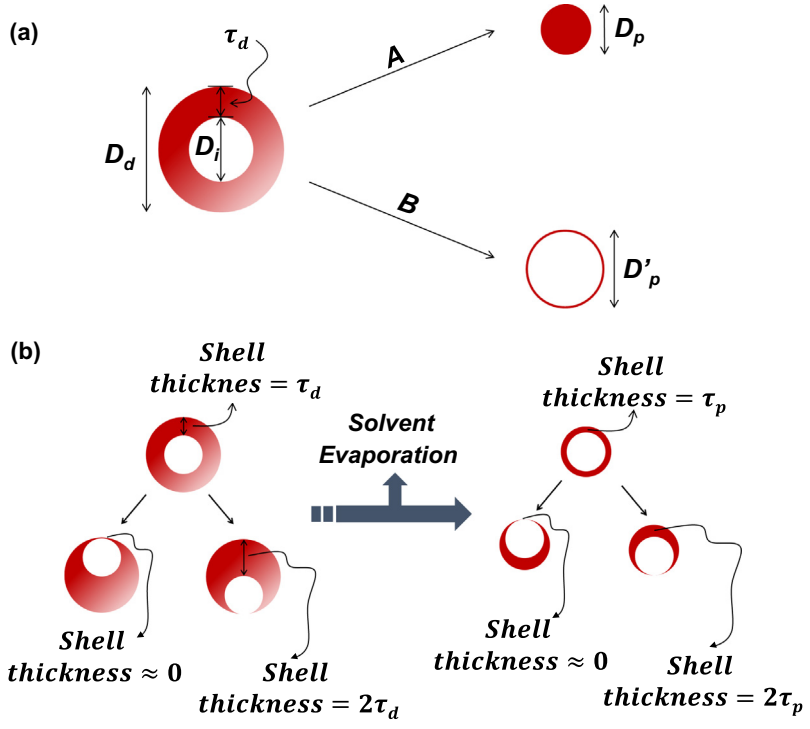

Fig. 2. (a) Particle formation by solvent evaporation from a core-shell drop with an inner diameter of D_i and an outer diameter of D_d. Path A: Evaporation with complete inner phase release. The resultant particle diameter is D_p; Path B: Evaporation with no inner phase release. The resultant particle diameter is $D'_p > D_p$. (b) Shell thickness variations as a result of different positions of the inner drop in core-shell drops/particles.

particle forming solids (PLA + PGPR) in the dispersed phase prior to solvent evaporation, and the initial diameters, D_i and D_d, of the inner and outer drop:

$$D_p = \sqrt[3]{x_p \frac{\rho_d}{\rho_p}(D_d^3 - D_i^3)} \quad (1)$$

For Path B, the resultant particle diameter D'_p can be estimated from the equation:

$$D'_p = \sqrt[3]{x_p \frac{\rho_d}{\rho_p}(D_d^3 - D_i^3) + D_i^3} \quad (2)$$

For core-shell drops with very thin shells, the particle shell thickness, τ_p, can be calculated from the equation:

$$\tau_p = \tau_d x_p \frac{\rho_d}{\rho_p}\frac{D_d^2}{D_p'^2} \quad (3)$$

The droplet shell thickness can be estimated from the flow rates of the middle and inner fluid, Q_m and Q_i, and the frequency of generation of outer drops, f [31,32]:

$$\tau_d = \frac{D_d - D_i}{2} = \frac{D_i}{2}\left[\left(1+\frac{Q_m}{Q_i}\right)^{1/3} - 1\right] = \left(\frac{3Q_i}{4\pi f}\right)^{1/3}\left[\left(1+\frac{Q_m}{Q_i}\right)^{1/3} - 1\right] \quad (4)$$

The shell thickness of the initial drop (τ_d) and the resultant particle (τ_p), at any location along the shell circumference, can vary between ≈0 and 2τ, depending on the position of the inner drop relative to the outer surface, as illustrated in Fig. 2(b). If the thickness of the shell is greater than $2\tau_p$ at any point on the particle circumference, it indicates the loss of inner water phase and/or the presence of pores in the shell.

3. Results and discussion

3.1. Morphological changes of core-shell capsules with pure water in the cores

The effects of osmotic stress on particle morphology were investigated by placing the produced core-shell particles in Milli-Q water or 5 wt% aqueous Eudragit solution for 14 days, as illustrated in Fig. 3. Using fluorescence microscopy, the particle shells stained with Nile red could easily be distinguished from the core.

Fig. 3a shows the effects of osmotic pressure on the morphology of core-shell particles containing Milli-Q water in the core over a period of 2 weeks. Here, two distinct types of morphologies were observed when the particles were placed in an isotonic solution, i.e. Milli-Q water (Type I) and in a hypertonic solution (5 wt% aqueous Eudragit solution) (Type II). The PLA shell of Type I particles stayed intact during solvent evaporation (Fig. 4a) and stable during 2-week storage. The particles were transparent and highly deformable, due to their thin shells. The non-spherical shape of some of the Type I particles in Fig. 4a occurred due to deformation of fragile PLA shells during particle sampling.

By comparing the core diameter of the parent drops and the stored particles, D_i and D_p', the water entrapment efficiency after 14 days of storage was found to be 96% implying high drop and particle stability. Fig. 4b and c shows FIB images of Type I core-shell particles. Based on the droplet shell thickness, τ_d, of 56 μm, the particle diameter, D_p', of 264 μm, and the droplet diameter, D_d, of 361 μm, the shell thickness, τ_p, of a particle with a centrally aligned core predicted from Eq. (3) was 10 μm. As shown in Fig. 2b, the shell thickness can have any value from approximately zero to $2\tau_p$, depending on the relative position of the core and the point on the circumference observed. From Fig. 4c, the shell thickness was 12 μm, which is $1.2\tau_p$. Hence, the observed shell thickness is within the predicted interval of $0 - 2\tau_p$. From the cross section shown in Fig. 4c, it can be seen that the PLA shell has internal pores, which is consistent with the porous structure of PLA particles reported earlier [16] and contributes to the increased shell thickness compared to that for a non-porous polymer matrix. The shell thickness of produced microparticles can easily be tuned using Eq. (3) and the polymer forming the shell can be reinforced using biocompatible inorganic nanofillers such as nanoclay [16].

On the other hand, core-shell capsules with pure water in the core and stored in a hypertonic solution (Type II) were unstable and shrank with time. As shown in Fig. 4d and e, the particles progressively changed their morphology from buckled and dimpled shapes after day 2 (Fig. 4d) to crumpled morphologies after day 14 (Fig. 4e), which could be explained by the loss of inner water due to osmotic migration through the shell. It is well known that water can permeate through voids that exist in the amorphous regions of polymer films [33]. The osmotic stress-induced shrinkage serves as a further evidence of the water entrapment ability of our thin-shelled capsules. When Type I particles were exposed to ambient air, they lost their entrapped water and assumed a collapsed morphology due to deformation of the elastic shells.

3.2. Morphological changes of core-shell particles with Eudragit solution in the cores

Fig. 3b summarises the effect of storage conditions on the morphology of core-shell particles containing 5 wt% Eudragit solution in the core. Here, four distinct particle morphologies were observed when the particles were stored in an isotonic environment (5 wt% Eudragit solution) (Type III), in a hypotonic solution at pH ≈ 7 (Milli-Q water) (Type IV), in a hypotonic solution at pH ≈ 4 (10^{-4} M HCl solution) (Type V), and when the particles were dried after being stored in a hypotonic solution at pH ≈ 4 (Type VI).

Type III particles (Fig. 5(a-b)) had the same morphology and stability as Type I particles due to isotonic environments in both cases. The distinctive 'pea-like' eyes on the transparent particle shells are evaporated satellite oil droplets formed during microfluidic drop generation which are unavoidable and have been predicted in our recent numerical simulation study [34]. After 2 days of storage, the diameter of Type IV particles was 8% larger than the diameter of Type III particles, due to an inward flux of water caused by hypotonic environment. This influx of water decreased the pH in the core solution thereby inducing partial aggregation of Eudragit chains, because the polymer was originally dissolved in 0.1 M NaOH at pH 13. As a result, the particles in Fig. 5c are less transparent than Type III particles in Fig. 5a and b. On prolonged storage, the particles became transparent with wrinkled surface (Fig. 5d) which was likely because of their burst as a result of built-up internal pressure.

Core-shell microcapsules with gelled aqueous cores. Type V particles were formed by placing the capsules in 10^{-4} M HCl solution, which caused an ionic gelation of the core solution due to the diffusion of H^+ ions through the shell and charge neutralisation of Eudragit chains. At pH > 7, Eudragit S 100 molecules are negatively charged due to deprotonation of carboxyl functional groups in methacrylic acid residues and thus, the polymer is soluble in water due to electrostatic repulsion between the chains (Fig. 3d). Due to the reversible transition of Eudragit from a hydrophilic to hydrophobic state at pH < 7, a homogeneous core solution underwent a phase separation into an Eudragit-rich region (dark eccentric cores in Fig. 5e) and a water-rich region (transparent, crescent-shaped regions next to the dark gel portions in Fig. 5e). Because Nile red is an uncharged and hydrophobic dye insoluble in water [35], the water-rich regions showed no red[1] colour on fluorescence images (Fig. 5f). On the other hand, gel regions showed red fluorescence (Fig. 5f) due to migration of the dye from the shell, confirming that Nile red can be used as a polarity-sensitive fluorescent probe of Eudragit hydrophobicity. The dark spots in the gel regions in Fig. 5f were caused by evaporated satellite droplets attached to the outer surface of the PLA shells.

Microcapsules with enteric polymer in the core can provide a pH-independent release profile of the drugs with a pH-dependent aqueous solubility, such as oxybutynin HCl. This drug is readily soluble in water at low pH values and sparingly soluble at high pH [36]. Although the drug is freely soluble in water at

[1] For interpretation of color in Fig. 5, the reader is referred to the web version of this article.

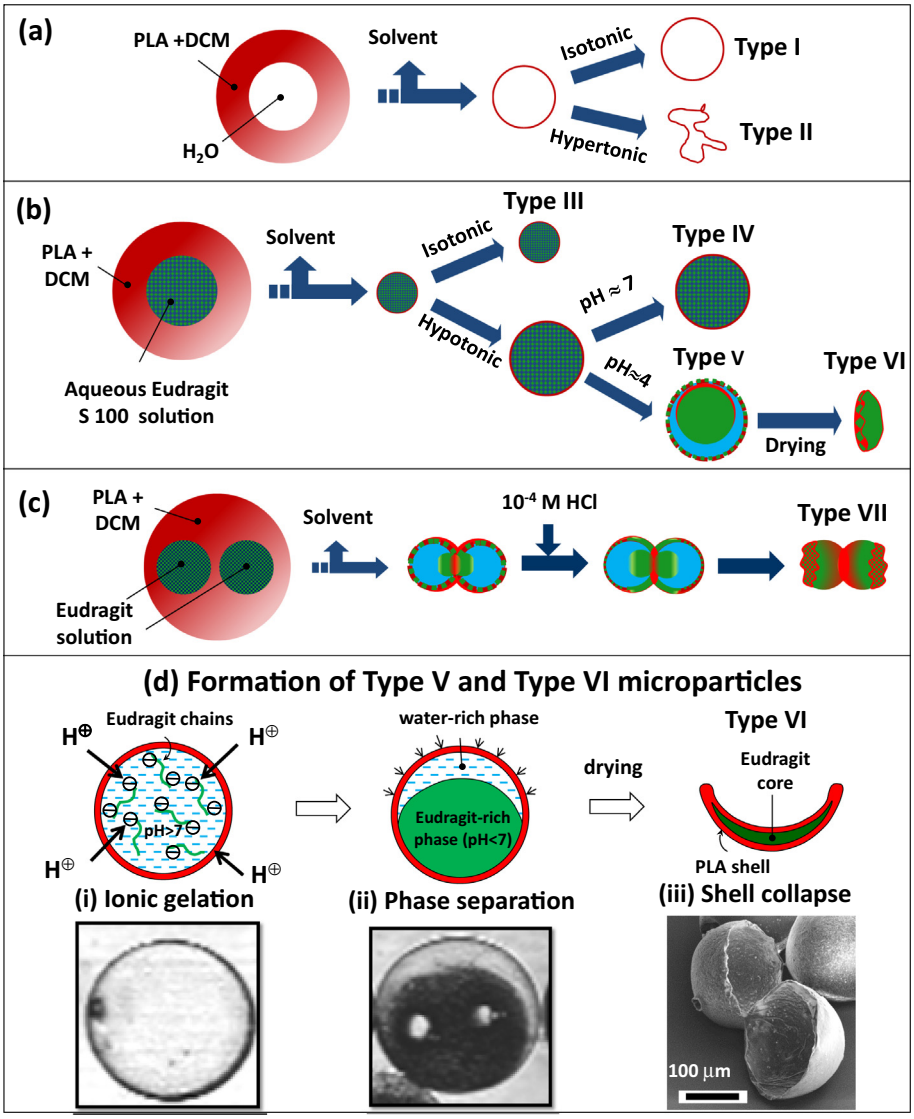

Fig. 3. Morphological changes of core-shell drops after solvent evaporation: (a) Capsule with Milli-Q water in the core stored in Milli-Q water (isotonic solution) (Type I) or 5 wt% aqueous Eudragit S 100 (hypertonic) solution (Type II); (b) Capsule with 5 wt% aqueous Eudragit solution in the core stored in 5 wt% aqueous Eudragit solution (Type III), a neutral hypotonic environment (Milli-Q water) (Type IV), or acidic hypotonic environment (10^{-4} M HCl) (Type V), and dried (Type VI); (c) Dual-core capsule with 5 wt% aqueous Eudragit solution in the cores stored in 10^{-4} M HCl and dried (Type VII); (d) Stages in the formation of composite crescent (Type VI) microparticles by the shell collapse along the interface between the shell surface and the water-rich crescent region shown by small arrows in figure (ii).

low pH, the diffusion is hindered by the formed gel network and the release rate is limited. At high pH values, the drug can easily diffuse out of the core due to gel disintegration, but the drug release is limited by the poor drug solubility. For drugs with pH-independent solubility profiles, the presence of a pH-sensitive gel in the core can provide a pH-triggered release. In the acidic environment of the stomach, the drug is immobilised within the gelled core and protected from the gastric acid. Many protein drugs are unstable in acidic environments and require protection from biocompatible excipients [37]. As the microcapsule reaches the intestine, the pH increases above the transition pH of the gel and the drug is released through the thin biodegradable shell.

Crescent-shaped microparticles. When Type V particles were dried at room temperature, crescent microparticles (Type VI) were formed (Fig. 5g-h) due to the collapse of a thin PLA shell encompassing the water-rich crescent domains in phase-separated cores. The shell indentation is a result of inferior mechanical properties of the PLA membrane during water evacuation. Fig. 5g is a FIB image of composite crescent particles composed of PLA shells and Eudragit® S 100 cores. The crescent particles were monodispersed and their radius of curvature was consistent with the size of the parent drops. Due to their hydrophilic core and hydrophobic outer surface, these particles could serve as microwells for hydrodynamic cell trapping and long-term cell analyses. The size of the cavity in the microwells can be controlled during drop generation to achieve single cell trapping and immobilisation.

Multicore-shell microcapsules with gelled aqueous cores. Type VII particles were formed by solvent evaporation of double core-single shell drops containing 5% aqueous Eudragit solution in the cores (Fig. 3c). The produced particles were stored in acidified water to trigger *in situ* gelation of Eudragit polymer. The thin PLA shell at opposite ends of the particles ruptured (Fig. 5i and j) as a result of the high influx of water from the outer aqueous phase into the cores via available surface area. The PLA shell did not collapse into spherical Type V particles (Fig. 5e and f), since the spherical shape gave rise to a uniform tension over the entire surface of

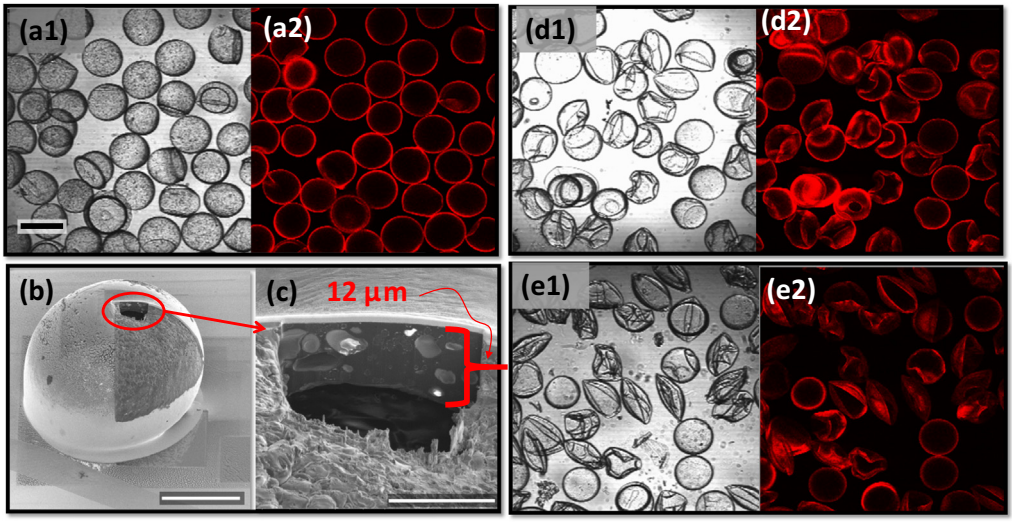

Fig. 4. (a-c) Micrographs of Type I particles: (a1) optical image; (a2) fluorescence image. (b-c) FIB images of a cross-sectioned particle. (d-e) Micrographs of Type II particles stored for (d) 2 days, (e) 14 days: (d1) & (e1) optical images; (d2) & (e2) fluorescence images. Scale bars: (a1-a2) 250 µm; (b) 100 µm; (c) 20 µm; (d-e) 200 µm.

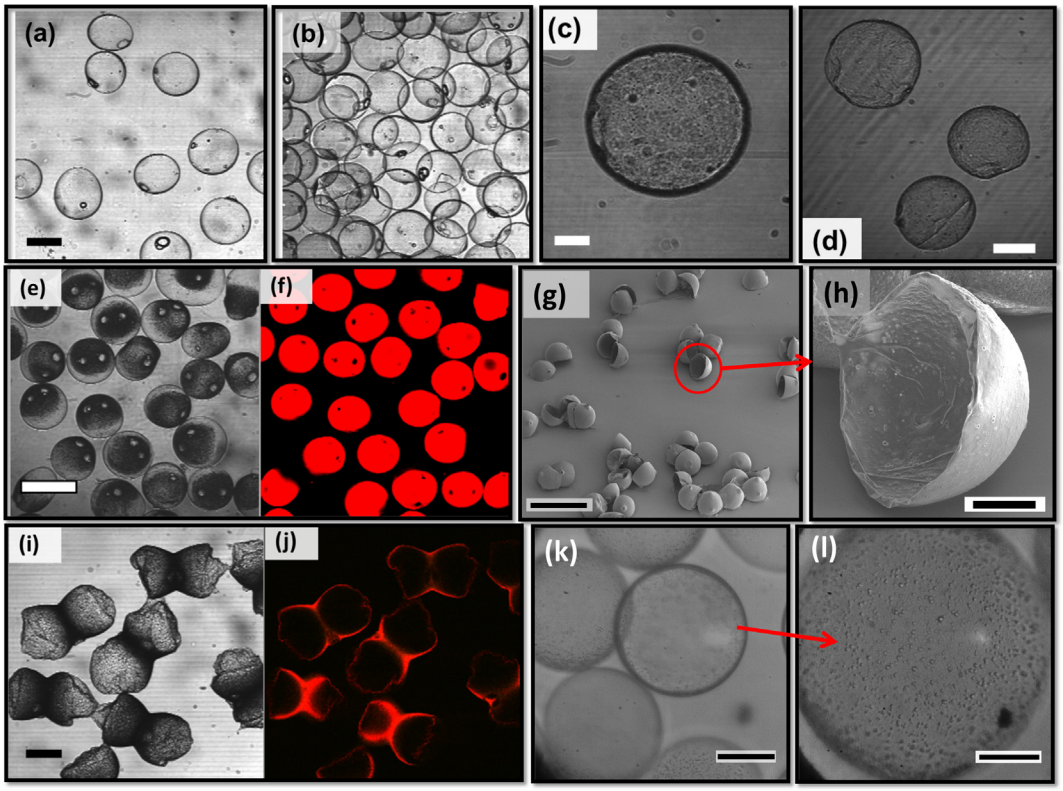

Fig. 5. Micrographs of composite particles: (a-b) Type III particles stored for: (a) 2 days, (b) 14 days. (c-d) Type IV particles stored for: (c) 2 days, (d) 14 days. (e-f) Type V particles: (e) optical image, (f) fluorescence image. (g-h) FIB images of Type VI particles. (i-j) Type VII particles: (i) optical image, (j) fluorescence image. (k-l) Core-shell particles with entrapped yeast cells. Scale bars: (a-b) 200 µm; (c) 50 µm; (d) 100 µm; (e-f) 300 µm; (g) 200 µm; (h) 100 µm; (i-j) 200 µm; (k) 150 µm; (l) 80 µm.

the PLA shell, unlike non-spherical particles with two cores. The resulting type VII particles have a morphology of two fused crescent particles.

3.3. Entrapment of yeast cells in core-shell microcapsules

The produced core-shell capsules can serve as disposable picolitre bioreactors for storage and culture of microbial cells. Fig. 5k and l show a successful entrapment of baker's yeast (*Saccharomyces cerevisiae*) cells with a diameter of 5–7 µm in the aqueous cores. The encapsulation efficiency was high with no yeast cells detected in the outer aqueous phase. In addition, the polymer shell was stable over prolonged incubation in an isotonic solution. The cell-loaded capsules can be dispersed in a culture medium to allow constant supply of nutrients and removal of metabolites through their semi-permeable shells. The diffusion rate of permeants can be controlled by changing the shell thickness and the cells can be released on demand by exposing the capsules to osmotic stress or applying a gentle rupture force.

4. Conclusions

Biodegradable synthetic polymer microcapsules of tuneable size, shape, and internal morphology have been produced through single-step microfluidic emulsification and subsequent solvent evaporation by varying the fluid flow rates, emulsion formulation, post-emulsification treatment, and incubation conditions. Core-shell morphology of the parent W/O/W emulsion drops remained intact during solvent evaporation, which resulted in the formation of core-shell capsules with a shell thickness of around 10 μm, entrapping the inner aqueous phase with 96% encapsulation efficiency. The shell retained its structural integrity after particle storage for two weeks in an isotonic solution, but buckling and crumbling of the particles occurred in a hypertonic solution. The produced core-shell microcapsules can serve as disposable picolitre bioreactors for cell culture [38], which was demonstrated by encapsulating baker's yeast cells in the aqueous cores. The cells can be released on demand by exposing the microcapsules to osmotic stress or applying a gentle rupture force.

Core-shell microcapsules with a gelled aqueous core and a biodegradable PLA shell were fabricated by an off-chip ionic gelation of a pH-sensitive polymer, Eudragit S 100, in the core. The gelation was achieved by placing the core-shell microcapsules in 10^{-4} M HCl solution, which caused the migration of H^+ ions from the outer aqueous phase through the shell and a reversible sol-gel transition of Eudragit. The transition of Eudragit from hydrophilic to hydrophobic state was confirmed by the redistribution of Nile red, a polarity-sensitive fluorescent probe [35] from the PLA shell to gelled region in the core. Microcapsules of similar architecture were obtained by templating W/O emulsions stabilised by polystyrene latex particles, followed by the formation of a cold-set gel in the aqueous core [39]. However, our method does not require the temperature control and multiple washing cycles with ethanol and water. The microcapsules with gelled aqueous cores are mechanically more robust than liquid-core capsules and enable a more extended release of hydrophilic actives by providing two levels of entrapment: the first level is provided by the gel matrix and the second level is provided by the PLA membrane encompassing the gel region.

In pharmaceutical formulations, Eudragit was typically used as an outer coat and biodegradable synthetic polymer formed a core [40]. In this work, Eudragit is incorporated in the core and PLA is a shell material, which leads to higher loading capacities of hydrophilic actives, because the core occupies the great majority of the capsule volume. In conventional matrix-type capsules, the loading capacity of hydrophilic actives is typically about 1% [40], because the volume fraction of the inner phase in the W_1/O emulsion is usually small, about 10%. The strategy of ionotropic gelation of aqueous cores developed in this study can be extended to alginate, chitosan, pectin, carboxymethyl cellulose, and other gel-forming polyelectrolytes and can be achieved using various divalent and polyvalent ions as cross-linkers instead of hydrogen ions.

Crescent microparticles were formed by drying the microcapsules consisting of phase-separated gelled cores at room temperature, due to collapse of the PLA shell encompassing a water-rich, crescent-shaped region during water evacuation. The produced crescent particles have a composite structure with PLA shells and Eudragit cores, and they differ from the crescent particles formed by polymerisation of Janus droplets composed of non-curable phase and photocurable phase [4,26] and selective polymer leaching from acorn-shaped Janus particles [1]. Crescent-shaped particles can be used as disposable, biocompatible microvials for cell trapping and analysis. The size of the cavity can be adjusted to achieve a single cell trapping.

Acknowledgements

E.E.E. holds a scholarship from Niger Delta Development Commission (NDDC), Nigeria. The authors gratefully acknowledge the financial support from the EPSRC – United Kingdom grant EP/HO29923/1 and the assistance of Scott Doak from the Loughborough Materials Characterisation Centre for the FIB imaging.

Appendix A. Supplementary material

Supplementary data associated with this article can be found, in the online version, at http://dx.doi.org/10.1016/j.jcis.2017.03.067.

References

[1] J.H. Kim, T.Y. Jeon, T.M. Choi, T.S. Shim, S.H. Kim, S.M. Yang, Droplet microfluidics for producing functional microparticles, Langmuir 30 (2014) 1473–1488, http://dx.doi.org/10.1021/la403220p.
[2] J. Zhu, R.C. Hayward, Hierarchically structured microparticles formed by interfacial instabilities of emulsion droplets containing amphiphilic block copolymers, Angew. Chem., Int. Ed. 47 (2008) 2113–2116, http://dx.doi.org/10.1002/anie.200704863.
[3] B. Wang, H.C. Shum, D.A. Weitz, Fabrication of monodisperse toroidal particles by polymer solidification in microfluidics, ChemPhysChem 10 (2009) 641–645, http://dx.doi.org/10.1002/cphc.200800786.
[4] W. Lan, S. Li, J. Xu, G. Luo, A one-step microfluidic approach for controllable preparation of nanoparticle-coated patchy microparticles, Microfluid. Nanofluid. 13 (2012) 491–498, http://dx.doi.org/10.1007/s10404-012-0984-9.
[5] K.H. Hwangbo, M.R. Kim, C.S. Lee, K.Y. Cho, Facile fabrication of uniform golf-ball-shaped microparticles from various polymers, Soft Matter 7 (2011) 10874, http://dx.doi.org/10.1039/c1sm06529g.
[6] D. Lee, D.A. Weitz, Nonspherical colloidosomes with multiple compartments from double emulsions, Small 5 (2009) 1932–1935, http://dx.doi.org/10.1002/smll.200900357.
[7] H.C. Shum, Y. Zhao, S.H. Kim, D.A. Weitz, Multicompartment polymersomes from double emulsions, Angew. Chem., Int. Ed. 50 (2011) 1648–1651, http://dx.doi.org/10.1002/anie.201006023.
[8] N.N. Deng, M. Yelleswarapu, W.T.S. Huck, Monodisperse uni- and multicompartment liposomes, J. Am. Chem. Soc. 138 (2016) 7584–7591, http://dx.doi.org/10.1021/jacs.6b02107.
[9] N.G. Min, M. Ku, J. Yang, S.H. Kim, Microfluidic production of uniform microcarriers with multicompartments through phase separation in emulsion drops, Chem. Mater. 28 (2016) 1430–1438, http://dx.doi.org/10.1021/acs.chemmater.5b04798.
[10] T. Nisisako, T. Ando, T. Hatsuzawa, Capillary-assisted fabrication of biconcave polymeric microlenses from microfluidic ternary emulsion droplets, Small 10 (2014) 5116–5125, http://dx.doi.org/10.1002/smll.201401269.
[11] X.Y. Ling, I.Y. Phang, C. Acikgoz, M.D. Yilmaz, M.A. Hempenius, G.J. Vancso, J. Huskens, Janus particles with controllable patchiness and their chemical functionalization and supramolecular assembly, Angew. Chem., Int. Ed. 48 (2009) 7677–7682, http://dx.doi.org/10.1002/anie.200903579.
[12] J. Flemke, M. Maywald, V. Sieber, Encapsulation of living *E. coli* cells in hollow polymer microspheres of highly defined size, Biomacromolecules 14 (2013) 207–214, http://dx.doi.org/10.1021/bm3016362.
[13] L. Ge, S. Lu, J. Han, R. Guo, Anisotropic particles templated by Janus emulsion, Chem. Commun. 51 (2015) 7432–7434, http://dx.doi.org/10.1039/C5CC00935A.
[14] G.T. Vladisavljević, Recent advances in the production of controllable multiple emulsions using microfabricated devices, Particuology 24 (2016) 1–17, http://dx.doi.org/10.1016/j.partic.2015.10.001.
[15] W.J. Duncanson, T. Lin, A.R. Abate, S. Seiffert, R.K. Shah, D.A. Weitz, Microfluidic synthesis of advanced microparticles for encapsulation and controlled release, Lab Chip 12 (2012) 2135–2145, http://dx.doi.org/10.1039/c2lc21164e.
[16] E.E. Ekanem, S.A. Nabavi, G.T. Vladisavljević, S. Gu, Structured biodegradable polymeric microparticles for drug delivery produced using flow focusing glass microfluidic devices, ACS Appl. Mater. Interfaces 7 (2015) 23132–23143, http://dx.doi.org/10.1021/acsami.5b06943.
[17] T.Y. Lee, R. Praveenkumar, Y.-K. Oh, K. Lee, S.-H. Kim, Alginate microgels created by selective coalescence between core drops paired with an ultrathin shell, J. Mater. Chem. B 4 (2016) 3232–3238, http://dx.doi.org/10.1039/C6TB00580B.
[18] C.H. Choi, J.H. Jung, Y.W. Rhee, D.P. Kim, S.E. Shim, C.S. Lee, Generation of monodisperse alginate microbeads and in situ encapsulation of cell in microfluidic device, Biomed. Microdevices 9 (2007) 855–862, http://dx.doi.org/10.1007/s10544-007-9098-7.
[19] A.G. Håti, D.C. Bassett, J.M. Ribe, P. Sikorski, D.A. Weitz, B.T. Stokke, Versatile, cell and chip friendly method to gel alginate in microfluidic devices, Lab Chip 16 (2016) 3718–3727, http://dx.doi.org/10.1039/C6LC00769D.
[20] S. Akbari, T. Pirbodaghi, Microfluidic encapsulation of cells in alginate particles via an improved internal gelation approach, Microfluid. Nanofluidics. (2013) 1–5, http://dx.doi.org/10.1007/s10404-013-1264-z.

[21] J.L. Madrigal, R.S. Stilhano, C. Siltanen, K. Tanaka, S.N. Rezvani, R.P. Morgan, A. Revzin, S.W. Han, E.A. Silva, Microfluidic generation of alginate microgels for the controlled delivery of lentivectors, J. Mater. Chem. B 4 (2016) 6989–6999, http://dx.doi.org/10.1039/C6TB02150F.
[22] C. Kim, S. Chung, Y.E. Kim, K.S. Lee, S.H. Lee, K.W. Oh, J.Y. Kang, Generation of core-shell microcapsules with three-dimensional focusing device for efficient formation of cell spheroid, Lab Chip 11 (2011) 246–252, http://dx.doi.org/10.1039/c0lc00036a.
[23] D. Velasco, E. Tumarkin, E. Kumacheva, Microfluidic encapsulation of cells in polymer microgels, Small 8 (2012) 1633–1642, http://dx.doi.org/10.1002/smll.201102464.
[24] P.W. Ren, X.J. Ju, R. Xie, L.Y. Chu, Monodisperse alginate microcapsules with oil core generated from a microfluidic device, J. Colloid Interface Sci. 343 (2010) 392–395, http://dx.doi.org/10.1016/j.jcis.2009.11.007.
[25] L. Liu, F. Wu, X.J. Ju, R. Xie, W. Wang, C. Hui Niu, L.Y. Chu, Preparation of monodisperse calcium alginate microcapsules via internal gelation in microfluidic-generated double emulsions, J. Colloid Interface Sci. 404 (2013) 85–90, http://dx.doi.org/10.1016/j.jcis.2013.04.044.
[26] S.H. Kim, A. Abbaspourrad, D.A. Weitz, Aphiphilic crescent-moon-shaped microparticles formed by selective adsorption of colloids, J. Am. Chem. Soc. 133 (2011) 5516–5524, http://dx.doi.org/10.1021/ja200139w.
[27] S.W. Kim, K.H. Hwangbo, J.H. Lee, K.Y. Cho, Microfluidic fabrication of microparticles with multiple structures from a biodegradable polymer blend, RSC Adv. 4 (2014) 46536–46540, http://dx.doi.org/10.1039/C4RA05864J.
[28] N.G. Min, B. Kim, T.Y. Lee, D. Kim, D.C. Lee, S.H. Kim, Anisotropic microparticles created by phase separation of polymer blends confined in monodisperse emulsion drops, Langmuir 31 (2015) 937–943, http://dx.doi.org/10.1021/la504385z.
[29] S.A. Nabavi, G.T. Vladisavljević, S. Gu, E.E. Ekanem, Double emulsion production in glass capillary microfluidic device: parametric investigation of droplet generation behaviour, Chem. Eng. Sci. 130 (2015) 183–196, http://dx.doi.org/10.1016/j.ces.2015.03.004.
[30] S.A. Nabavi, G.T. Vladisavljević, V. Manović, Semipermeable elastic microcapsules for gas capture and sensing, Langmuir 32 (2016) 9826–9835, http://dx.doi.org/10.1021/acs.langmuir.6b02420.
[31] P.W. Chen, R.M. Erb, A.R. Studart, Designer polymer-based microcapsules made using microfluidics, Langmuir 28 (2012) 144–152, http://dx.doi.org/10.1021/la203088u.
[32] G.T. Vladisavljević, H.C. Shum, D.A. Weitz, Control over the shell thickness of core/shell drops in three-phase glass capillary devices, Prog. Colloid Polym. Sci. 139 (2012) 115–118, http://dx.doi.org/10.1007/978-3-642-28974-3_20.
[33] J.R. Scherer, B.A. Bolton, Water in polymer membranes. 5. On the existence of pores and voids, J. Phys. Chem. 89 (1985) 3535–3540, http://dx.doi.org/10.1021/j100262a022.
[34] S.A. Nabavi, S. Gu, G.T. Vladisavljević, E.E. Ekanem, Dynamics of double emulsion break-up in three phase glass capillary microfluidic devices, J. Colloid Interface Sci. 450 (2015) 279–287, http://dx.doi.org/10.1016/j.jcis.2015.03.032.
[35] D.L. Sackett, J. Wolff, Nile red as a polarity-sensitive fluorescent probe of hydrophobic protein surfaces, Anal. Biochem. 167 (1987) 228–234, http://dx.doi.org/10.1016/0003-2697(87)90157-6.
[36] X. Wen, A. Nokhodchi, A. Rajabi-Siahboomi, Oral extended release hydrophilic matrices: formulation and design, in: H. Wen, K. Park (Eds.), Oral Controlled Release Formulation and Drug Delivery: Theory and Practice, John Wiley & Sons, Hoboken, 2010, pp. 89–100.
[37] V. Jain, D. Prasad, D. Jain, S.K. Mishra, R. Singh, Factorial design-based development of measlamine microspheres for colonic delivery, Biomaterials 1 (2011) 182–188, http://dx.doi.org/10.4161/biom.18461.
[38] W. Zhang, S. Zhao, W. Rao, J. Snyder, J.K. Choi, J. Wang, I.A. Khan, N.B. Saleh, P.J. Mohler, J. Yu, T.J. Hund, C. Tang, X. He, A novel core-shell microcapsule for encapsulation and 3D culture of embryonic stem cells, J. Mater. Chem. B 1 (2013) 1002–1009, http://dx.doi.org/10.1039/c2tb00058j.
[39] O.J. Cayre, P.F. Noble, V.N. Paunov, Fabrication of novel colloidosome microcapsules with gelled aqueous cores, J. Mater. Chem. 14 (2004) 3351–3355, http://dx.doi.org/10.1039/b411359d.
[40] P.C. Naha, V. Kanchan, P.K. Manna, A.K. Panda, Improved bioavailability of orally delivered insulin using Eudragit-L30D coated PLGA microparticles, J. Microencapsul. 25 (2008) 248–256, http://dx.doi.org/10.1080/02652040801903843.